HHS Public Access

Author manuscript

*Combust Flame*. Author manuscript; available in PMC 2016 July 25.

Published in final edited form as:

*Combust Flame*. 2016 May ; 167: 218–227.

# Potential Explosion Hazard of Carbonaceous Nanoparticles: Screening of Allotropes

**Leonid A. Turkevich**[*],
National Institute for Occupational Safety and Health, Division of Applied Research and Technology, 1090 Tusculum Avenue, MS-R7, Cincinnati, OH 45226 USA

**Joseph Fernback**,
National Institute for Occupational Safety and Health, Division of Applied Research and Technology, 1090 Tusculum Avenue, MS-R7, Cincinnati, OH 45226 USA

**Ashok G. Dastidar**, and
Fauske & Associates, LLC, 16W070 83rd Street, Burr Ridge, IL 60527 USA

**Paul Osterberg**
Fauske & Associates, LLC, 16W070 83rd Street, Burr Ridge, IL 60527 USA

## Abstract

There is a concern that engineered carbon nanoparticles, when manufactured on an industrial scale, will pose an explosion hazard. Explosion testing has been performed on 20 codes of carbonaceous powders. These include several different codes of SWCNTs (single-walled carbon nanotubes), MWCNTs (multi-walled carbon nanotubes) and CNFs (carbon nanofibers), graphene, diamond, fullerene, as well as several different control carbon blacks and graphites. Explosion screening was performed in a 20 L explosion chamber (ASTM E1226 protocol), at a concentration of 500 g/m$^3$, using a 5 kJ ignition source. Time traces of overpressure were recorded. Samples typically exhibited overpressures of 5–7 bar, and deflagration index $K_{St} = V^{1/3} (dP/dt)_{max} \sim 10 –$ 80 bar-m/s, which places these materials in European Dust Explosion Class St-1. There is minimal variation between these different materials. The explosive characteristics of these carbonaceous powders are uncorrelated with primary particle size (BET specific surface area).

### Keywords

explosion hazard; dust; carbon; nanoparticle; nanomaterials

[*]corresponding author: LLT0@cdc.gov (Leonid Turkevich).

**Disclaimers**

The findings and conclusions in this report are those of the authors and do not necessarily represent the views of the National Institute for Occupational Safety and Health. Mention of product or company name does not constitute endorsement by the Centers for Disease Control and Prevention.

None of the authors has a financial relationship with a commercial entity that has an interest in the subject of this manuscript.

# 1. Introduction

Under certain conditions, engineered nanomaterials may pose a dust explosion hazard. Some nanoparticles may even spontaneously ignite when exposed to air [1] or to light [2]. Very little is known about the potential explosivity of materials when subdivided down to the nano-scale.

This is the first of two articles describing our work on carbonaceous nanomaterials. This first article reports on our survey of carbonaceous allotropes to screen for their potential explosivity. A second article [3] reports on detailed explosion parameter measurements on selected materials.

We have measured explosion parameters of several carbon nanomaterials: fullerene, single-walled carbon nanotubes (SWCNTs), multi-walled carbon nanotubes (MWCNTs), carbon nanofibers (CNFs), carbon blacks, graphites, graphene, diamond. Such measurements have not been previously made. Explosion experiments were conducted in a 20-L chamber that has been utilized extensively to characterize the explosion characteristics of coal dust. Attempt is made to correlate these explosion parameter measurements with specific surface area. Measured parameters include maximum explosion pressure, $P_m$, and explosion severity index, $K = dP/dt|_m \, V^{1/3}$, derived from the maximum rate of pressure rise, $dP/dt|_m$.

## 1.1 Introductory Remarks

A dust explosion may occur as the result of dust particles being suspended in the air under confinement and exposed to an ignition source [4–6]. Most organic materials, if finely divided and dispersed in air, will explode if ignited by a sufficiently strong ignition source [5].

Industrial dust explosions have been documented since the 1785 Giacomelli flour warehouse explosion in Turin [7, 5]. More recent dust explosions have resultedin significant property damage, injury and loss of life (e.g. 2008 Imperial Sugar explosion, Port Wentworth, GA [8]; 2010 Upper Big Branch Mine coal dust explosion, Montcoal, WV [9]).

Over the past decade, nanomaterials (ultra-fines) have been the subject of extensive research due to their enhanced properties, some of which derive from their large specific surface area [10]. As the production and use of nanomaterials increase (e.g. industrial production of carbon nanotubes [11–13]), associated risks will also increase. Knowledge about the physico-chemical hazards related to these new materials remains limited [14], in particular, the potential for dust explosion [15–16]. This raises the concern of the potential hazard of nanopowder fires and explosions [17–18], Explosion hazards may exist for processes such as mixing, grinding, drilling, sanding, and cleaning [19–21].

## 1.2 Previous Work

**1.2.1. Overview—**Dust explosion texts [4–5] do not discuss the explosion of powders of particles smaller than 10 μm. The IFA explosion database [22] lists dust explosivity test data only for micrometer-sized powders. A literature review [18] of the explosion and flammability hazards of nanopowders again primarily discusses micrometer-sized powders.

Nanomaterial explosibility data thus remain limited. It is unknown whether extrapolation of explosion and flammability studies from micron-sized powders to nanopowders is valid.

Two classes of nanomaterials have elicited the most attention: carbonaceous nanoparticles and metallic nanoparticles. The nano-metals exhibit more severe explosions than do the nano-carbons [21, 1]. However, the chemical reaction pathway for metallic nanoparticle explosion is qualitatively different from the pathway for carbon nanoparticle explosion, and it is an oversimplification to treat both classes interchangeably. This paper focuses exclusively on the measurement of the explosion parameters for carbonaceous nanomaterials.

In 1845, Faraday and Lyell [23] suggested that coal dust could provide additional fuel for colliery explosions initiated by methane gas ignition. There is an extensive literature on coal dust explosion parameters (Supplemental Material). Particle sizing was rarely attempted in the early experiments, although the later studies [24–25] can be extrapolated to zero particle size. Typically, $P_{max}$ ~ 6 – 7 bar, $K_{St}$ ~ 40 – 60 m-bar/s, MEC ~ 60–200 g/m$^3$, MIE ~ 30 – 200 mJ, and $MIT_{cloud}$ ~ 450 – 1100°C.

Explosion studies have also been conducted on several pure carbon systems: carbon blacks [26–28] and graphite [29–30]. For most of these materials, $P_{max}$ ~ 6 – 8 bar, $K_{St}$ ~ 10 – 140 m-bar/s, MEC ~ 40 – 150 g/m$^3$, MIT ~ 650 – 900°C, comparable to the coals; a nonrigorous lower bound of MIE ~ 1 mJ would be considerably lower than that of the coals.

**1.2.2. Recent Nanopowder Work—**Using the standard 20 L explosion sphere [31], Vignes et al. [14] assessed the explosion severity ($P_{max}$, $K_{St}$) and explosion sensitivity (MIE, MEC) of various carbon black powders (Corax N115, Thermal Black N990, Corax N550, Printex XE2), and one unidentified carbon nanotube (which we believe to be an Arkema MWCNT). These Nanosafe2 results have been reported in several places [32–33], not always with identical values. Bouillard et al. [32, 34–35] observed that carbon nanopowders exhibit a low propensity to explode while metallic nanopowders can be very reactive; they, therefore, highlighted the high potential for explosion risks of only the metallic nanoparticles in manufacturing facilities. The explosion parameters for the carbon materials from the NanoSafe 2 studies are included in Table 1, where, for several of the entries, we have chosen the most likely of the reported values.

Work has also been done, using a (non-standard) smaller 2 L chamber, on several allotropes of carbon: MWCNT, CNF and carbon black [36]. The explosion parameters, as measured in this smaller chamber, are suspect, since the proximity of the quenching external surface acts as a heat sink and will tend to suppress any developing explosion (§ 4.4). Vignes et al. [14] and Dufaud et al. [16] have questioned the applicability of even the larger 20 L sphere data to assess the risk from nanopowders. Hence, the explosion parameters from the 2 L chamber studies have not been included in Table 1.

Worsfold et al. [21] review uncritically the results on the explosibility of nanomaterials, with data taken mainly from the Nanosafe2 project.

### 1.2.3. Previous Results on the Size-Dependence of Explosion Parameters

**1.2.3.1. Explosion severity:** In general, as particle size decreases (and the specific surface area increases), the explosion severity, as indicated by $P_{max}$, and $(dP/dt)_{max}$, increases. However, for the few materials studied, as the particle size is reduced below ~ 50 μm, severity ceases to increase. This quasi-plateau has been attributed variously to particle agglomeration and/or reaction mechanisms.

For coal, as the particle size is decreased, there is no further increase in either $P_{max}$ or $(dP/dt)_{max}$ below ~ 50 μm [5]. Similarly, $P_{max}$ exhibits a plateau at particle sizes < 50 μm for flour and < 40 μm for methylcellulose [37–38]. For polyethylene, $P_{max}$ exhibits a plateau for particle sizes < 50 μm [37–38]. Polyvinyl chloride (PVC) behaves differently: $P_{max}$ continues to increase in the particle size range 25 – 150 μm. Explosion severities ($P_{max}$, $K_{St}$) for the uncharacterized NanoSafe CNTs are comparable to those found for coals and nanostructured carbon blacks.

**1.2.3.2. Other Explosion parameters:** Discussion of minimum explosive concentration (MEC), minimum ignition energy (MIE) and minimum ignition temperature (MIT) is discussed in [3].

### 1.2.4 Possible Origin of a Limiting Particle Size

**1.2.4.1. Limiting Particle Size arising from Reaction Mechanism:** A limiting particle size can be understood in the context of the various steps in the reaction mechanism [39]. In the case of a coal dust explosion (or any other organic material), combustion primarily occurs in the homogeneous gas phase. The combustion rate of the dust cloud depends on the relative time constants of the three processes: devolatilization, gas phase mixing and combustion. Particle size primarily influences the devolatilization rate; a higher specific area allows more rapid devolatilization. However, if gas phase combustion is the rate limiting step, increasing the devolatilization rate (by decreasing the particle size) will not increase the overall combustion rate.

For the case of coal, the maximum explosive severity is achieved for particle size ~ 50 μm; smaller, micron-sized coal particles do not further increase the severity. The particles must undergo heating, melting, devolatilization, and the combustion reaction occurs in the gas phase. For sub-micron coal particles, the heating, melting and vaporization processes occur more quickly than the gas phase reaction process, which latter becomes the rate determining step. The severity of a nano-coal dust explosion is not expected to increase because the rate limiting step is the vapor combustion [18, 15].

Intrinsically stable carbon allotropes may have more inhibited devolatilization; thus a smaller particle size might be needed for the devolatilization rate to compete with the combustion reaction rate.

**1.2.4.2. Limiting Particle Size arising from Agglomeration:** The possibility [21] that agglomeration reduces the explosion severity of nanosized particles is discounted in [3].

## 2. Experimental Methods

Explosion experiments were conducted at Fauske & Associates, LLC (Burr Ridge, IL). BET specific surface areas were measured at Pacific Surface Science (Ventura, CA). Transmission electron microscopy (TEM) was performed at the NIOSH Alice Hamilton Lab (Cincinnati, OH).

### 2.1 Qualitative Explosion Screening

The 1.2-L Hartmann tube [40–41] is often used for preliminary screening tests. However, it may yield false negatives for dusts that are difficult to ignite with a spark but that are ignitable with stronger ignition sources. It is not recommended [31] for measuring rates of pressure rise.

For several limited quantity materials, we used the Hartmann tube to assess their explosion potential: i) fullerene soot; ii) SWCNT-Unidym P0261, oven dried; iii) SWCNT-Unidym R0513 hexane extracted and heat dried; iv) SWeNT SWCNT; v) CheapTubes SWCNT.

### 2.2 Quantitative Explosion Severity Test ($P_{max}$, $dP/dt|_{max}$, $K_{max}$)

The test method [31] provides a laboratory procedure to evaluate deflagration parameters of dusts. The parameters measured are the maximum overpressure, $P_{max}$, and the maximum rate of pressure rise, $dP/dt|_{max}$, scaled to a standard 1-$m^3$ containment vessel: $K_{St} = V^{1/3} (dP/dt)_{max}$, where V is the volume of the explosion chamber [4, 43]. The acquisition, use, and limitations of $K_{St}$ data have been discussed in [42].

The tests were conducted in a spherical, stainless steel 20-L Siwek chamber [4, 43–45] (manufactured by Adolf Kuehner AG, Basel, Switz.), outfitted with a rebound nozzle. While the level of dispersion in the 20-L chamber is comparable to that in the 1-$m^3$ apparatus [45a,b], the two chambers exhibit differences in turbulence decay [45c,d]. In addition, the cube-root scaling for $K_{St}$ is only valid in the limit of infinitesimal flame thickness [45c–e].

Ignition was effected with a single 5 kJ Sobbe source (electrically activated, pyrotechnic ignitor, containing 40% zirconium metal, 30% barium nitrate, 30% barium peroxide—manufactured by Fr. Sobbe GmbH, Dortmund, Germany), located at the center of the sphere; while the usual screening test uses two such sources, we were concerned that 10 kJ would overdrive the explosion. In fact, a single 5 kJ igniter may overdrive these explosions [45f–i]; for a discussion of the interaction of a strong ignition source with initial turbulence, see [45j]. The energy is the nominal calorimetric value (based on the mass of pyrotechnic powder in the ignitor). The 5 kJ ignitor by itself produces a pressure rise of ~ 0.8 bar in the 20-L chamber (see below). The Sobbe ignitors are much more energetic than the electric sparks typically used in the 1.2-L Hartmann tube tests (hence the potential for false negatives in Hartmann tube screening).

### 2.3 Quantitative Explosion Screening

The screening test was performed at a nominal dust concentration c = 500 g/$m^3$ (the mass of loaded powder, 10 g, divided by the chamber volume, 20 L). This fuel-rich concentration is chosen so as to ensure an explosive event for an explosible material, even though this

explosion may not yield maximal explosion parameters. The explosion parameters are reported as $P_m(500)$, $K(500) = V^{1/3}\, dp/dt|_m(500)$

### 2.4 BET Specific Surface Area

BET specific surface areas [46–50] were determined using a TriStar II 3020 surface area and porosity measurement system (Micromeritics Instrument Corp., Norcross, GA). Adsorption of $N_2$ gas from a liquid nitrogen bath is measured at 5 pressures, P, relative to saturation, $P_0$: $P/P_0 = 0.05, 0.10, 0.15, 0.20, 0.25$. The BET fits (all with correlation coefficients $R^2 > 0.9986$) yield the specific surface area.

### 2.5 Electron Microscopy

**2.5.1 Sample preparation—**Each bulk powder sample was mechanically agitated in its vial. A lacy carbon TEM grid was then inserted into the vial, and the powder and TEM grid were shaken together. The TEM grid was then removed from the bulk powder, with a small residue of the powder adhering to the TEM grid.

**2.5.2 Microscopy—**The powder-laden TEM grids were examined on a JEOL field emission transmission electron microscope (model JEM-2100F, Akishima, Tokyo, Japan), equipped with STEM camera, operating at electron beam energy = 200 keV. Multiple images of each sample were obtained in bright field mode, at various magnifications (indicated in the figures).

### 2.6 Materials

Twenty powders were evaluated. Candidate materials included single-walled and multi-walled carbon nanotubes, carbon nanofibers, carbon blacks, fullerene, graphene, graphite, diamond. Detailed descriptions of these materials, their provenance and their properties, are provided in the Supplemental Material. Unless otherwise specified, materials parameters for the materials studied are those provided by the manufacturer.

## 3. Results

### 3.1 Visual determination of explosion by Hartmann tube

Several materials were visually evaluated for potential explosion hazard by experiments performed in a 1.2 L Hartmann tube. Figures 1 photographically document attempted explosions for four codes of SWCNT: a) Unidym (where explosive combustion is deemed to have occurred); b) hexane extracted Unidym (where no explosion is detected, with evidence of glowing embers from the large granules consolidated by the hexane extraction); c) SWeNT SG-65 (where no explosion is detected, and which is visually similar to cases in which the experiment is ‘fuel-starved’); d) CheapTubes (where no explosion is detected, with evidence of glowing embers). Figure 1 e) documents a similar explosion of fullerene soot, where no explosion is deemed to have occurred, the combustion being inefficient, with large quantities of ‘soot’ billowing from the top of the tube; however, with each attempted ignition, enough overpressure was generated to loft the Hartmann tube cover. Given the quantitative results for fullerenes (Table 2), we believe that the Hartmann tube explosions are initiated but are masked by the abundance of soot generated; the observed soot, in this

case, is primarily unexploded raw material and not the soot generated as the end product of the explosion (§ 4.6).

In summary, these Hartmann tube experiments are, at best, suggestive and, compared with the quantitative study (Table 2), sometimes misleading.

### 3.2 Explosion severity at c = 500 g/m$^3$ in Siwek chamber

Quantification of the severity of these carbonaceous explosions was conducted at nominal dust concentration c = 500 g/m$^3$, which represents fuel-rich (i.e. oxygen-limited) combustion. For each code, duplicate explosions were conducted, with very reproducible results; reported (Table 2) are the averages of the parameters obtained from these two runs.

A typical temporal pressure trace is shown in Figure 2a (shown is the case of CheapTubes SWCNT). The chamber is initially evacuated to P ~ −0.6 bar$_g$; the dust is introduced at t = 34 msec, and P → 0 bar$_g$. Ignition occurs at $t_{ign}$ = 93 msec; as the explosion develops, P rises rapidly (concave up), reaches (at $t_x$ = 124 msec) an inflection point (maximum $dP/dt|_m$), continues to rise (concave down), reaches (at t = 140 msec) a maximum pressure, $P_m$ = 6.8 bar$_g$. Since $t_x$ is roughly the time when the explosion front senses the chamber wall (and surface cooling becomes significant), the velocity of the explosion front may be estimated as $v \sim R/(t_x - t_{ign}) \sim 5.4$ m/sec, where R = 16.8 cm for the radius of the 20 L vessel.

The same data is re-plotted (Figure 2b) as $\log(P - P_0)$ vs. $\log(t - t_{ign})$. In the explosion region $0.8 < \log(t - t_{ign}) < 1.6$ (corresponding to 99 msec < t < 123 msec), the pressure develops algebraically. For large chambers, we expect [51–52] cubic evolution, $P(t) - P_0 \sim (t - t_{ign})^3$; in our experiments, we only see quadratic evolution. It is well-known (e.g. in critical phenomena) that fitting the slope in Fig 2b is very sensitive to the value of the parameter $t_{ign}$, and we also only have algebraic scaling over a limited range (less than a decade in the independent variable, t). This lack of cubic scaling is an additional argument against the use of still smaller (e.g. 2 L) chambers (q.v. § 4.4).

Reported in Table 2 are $P_m(500)$, $dP/dt|_m(500)$ and $K(500) = V^{1/3}\, dP/dt|_m(500)$ for the various materials, grouped by allotrope. A characteristic velocity of the explosion front can be constructed as $v \sim K/P_m$; for the CheapTubes SWCNT, this second estimate, v ~ 11.6 m/sec, is comparable to that derived above from the pressure trace.

### 3.3 Microscopy of exploded material

Following these screening experiments, we collected exploded material for examination under the electron microscope. Shown (Figures 3) are representative images from a)–b) MWCNT, c)–d) SWCNT, e) SDWeNT SWCNT, f) Unidym SWCNT (HiPCO process, g) graphene, h–i) fullerene, j) 10 nm diamond, k) carbon black (Printex 90), l) carbon black (Sterling V). In all cases, most of the material remains unexploded (90% – 95% of the fields examined); this is consistent with the screening experimental conditions being oxygen limited [3].

However, in all cases, we detected the presence of ‘soot balls’ in the exploded residue. The size of these soot balls varied between the different materials, as did their attachment to

features in the unexploded material. We cannot tell whether these soot balls originated at the locations that are captured in the micrographs, or whether the soot balls are generated elsewhere during the explosion (perhaps in the gaseous phase) and are only deposited on the unexploded material as the combustion cools, or even later, perhaps in the microscopy sample preparation process. We believe the ubiquity of these soot balls argues for a common mechanism for the explosive combustion of all these carbonaceous materials (q.v. § 4.6).

By contrast, electron micrographs of the post-explosion residue from Pittsburgh seam coal exhibit ‘blow holes’ [53]. These ‘blow holes’ provide direct evidence of the escape of volatile gases during the explosion process in that system. In our micrographs (Figure 3), we did not see any evidence of such ‘blow holes’, consistent with the absence of volatile gases in the carbonaceous nanoparticles.

### 3.4 Particle Size

For all the materials screened, primary particle size was measured by specific surface area, A, as derived from BET $N_2$ adsorption; these BET specific surface areas are reported in Table 2 (column 2), with estimated standard deviations, $\sigma_A$ (column 3).

## 4. Discussion

### 4.1 Overall Magnitudes of Explosion Parameters

All of these materials are very similar in their explosive behavior (Table 2). With the exception of the one carbon nanofiber (PR-24-XT-HHT), all of the materials exploded in the 20 L chamber under ignition energy of 5 kJ at c = 500 g/m$^3$ (We again caution that 5 kJ may be overdriving these explosions) Maximum explosion pressures are in the range 4.0 bar < $P_m(500)$ < 6.8 bar; these values are comparable to those of the coals and to the previously measured carbon blacks, although smaller than some of the earlier measured carbon blacks (Table 1). The explosion severity index of these nanocarbons is in the wider range 4 bar-m/sec < K(500) < 180 bar-m/sec; these values, again, are comparable to those of the coals and to those of the previously measured carbon blacks (Table 1). Thus, all these nanocarbon materials seem to reside in Explosion Class St-1, similar to cotton and wood dust [5,54].

In [3], we discuss the concentration variation of these explosions. In particular, as the fuel concentration is reduced, more optimal explosion conditions are achieved with slightly higher explosion overpressures and rates of pressure rise.

The one exceptional carbon nanofiber (PR-24-XT-HHT) that did not explode is peculiar in that, as the last manufacturing step, it has been exposed to a post-synthesis heat treatment [55]—the manufacturer believes that this heat treatment serves to ‘cap’ the ends of the rolled up tubes that constitute the nanofibers [55]. If the carbon atoms are preferentially liberated from the edges of the CNT, when this process is inhibited by end capping the tubes (as in PR-24-XT-HHT), the fuel source for the explosion is choked off as carbon atoms can no longer be provided to the gas phase. However, the same argument should inhibit the explosion of fullerene.

### 4.2 Particle Size Effects

For all of these materials, we have measured BET specific surface area, as an indicator of primary particle size. There appears to be no correlation (Figure 4a) between the strength of the explosion, $P_m(500)$, and the particle size (specific surface area); the material either explodes (at c = 500 g/m$^3$ and ignition energy = 5 kJ), or it does not, and the energy released in the oxidation of the carbon is very similar for all the different forms of carbon, i.e. $P_m(500)$ lies in a narrow band, irrespective of BET specific surface area. Similarly, the kinetics of the explosion, as measured by K(500), is uncorrelated with particle size (Figure 4b), i.e. K(500) vs. BET specific surface area is a scatter plot.

### 4.3 Allotrope Phase Map

The kinetics parameter, K(500), is strongly correlated with the thermodynamic parameter, $P_m(500)$, for these different allotropes of carbon (Figure 5). In addition, the allotropes appear to cluster together: graphite and CNF to the left (low $P_m(500)$, low K(500)), MWCNT and carbon black in the middle (mid-range $P_m(500)$ and mid-range K(500)), and diamond, SWCNT, fullerene to the right (high $P_m(500)$, high K(500)).

### 4.4 Effect of Explosion Chamber Volume

Our explosions are conducted in the 20 L Siwek chamber. HSE (UK Health Safety Executive) has performed similar measurements in a smaller 2 L chamber [36]. We believe those results are compromised due to the increased effect of surface cooling in that smaller chamber. In our experiments, the time dependence of the pressure at the chamber surface exhibits (Figure 2b) algebraic scaling, $P - P_0 \sim (t - t_{ign})^2$, in the intermediate regime $0.9 < \log(t - t_{ign}) < 1.5$, which differs from the expected [52] cubic time dependence for an explosion developing in an unconfined space. Deviations from algebraic scaling occur, at the earlier times, due to the initial ignition conditions, and, at the later times, due to cooling by the metal surface of the chamber. The cross-over, at $t_x$, to cooling-dominated behavior occurs roughly when dP/dt is maximized; at time $t_x$, the explosion front begins to sense the presence of the metal surface heat sink. By reducing the explosion chamber volume, this cross-over time, $t_x$, is reduced ($t_x - t_{ign} \sim 30$ msec for 20 L to $t_x - t_{ign} \sim 16$ msec for 2 L), and the algebraic scaling regime is reduced to $0.9 < \log(t - t_{ign}) < 1.2$ (since the induction time for the explosion to develop is not changed). We argue that it is not reliable to estimate $dP/dt|_m$ from such a limited scaling regime. In fact, experiments in the 20-L chamber may underestimate $K_{St}$ [45c]

### 4.5 Aggregation Effects

We believe that aggregation of the primary particles is not a significant determinant of the explosion parameters. This is discussed in detail in [3].

### 4.6 Explosion Mechanism

We believe that the electron micrographs of the exploded material suggest a common explosion pathway for these materials. Carbon atoms are released from the solid particles, and the oxidation reaction takes place in the gas phase. At high temperatures, the reaction $2\ C + O_2 \rightarrow 2\ CO$ is favored [56] over the reaction $C + O_2 \rightarrow CO_2$. Following the reaction, as

the system cools, the CO disproportionates [57] (Boudouard reaction), 2 CO → C (soot) + $CO_2$. The reaction mechanism is universal; hence the ubiquity of the soot balls observed in the electron micrographs of the exploded material.

The structure of the solid carbon fuel has two effects. The different allotropes of carbon have slightly different heats of fusion, resulting in slight differences in the thermodynamics of the explosion; thus all the materials have comparable values of $P_m(500)$, but there is a tendency for $P_m(500)$ to be clustered by allotrope (Figure 5). Similarly, difference in the activation energy to release the carbon atoms off of the solid particulates will result in a slight difference in kinetics; again, there is a tendency for $K_{St}(500)$ to be clustered by allotrope (Figure 5).

The composition of Carbon vapor is known to be nontrivial. Carbon cluster ions were originally detected in vapor produced from high frequency arc graphite electrodes [58a,b]. A sufficient number of small carbon clusters are in equilibrium in the vapor and have a major effect on the heat of sublimation [58c,d,e]. Their presence [58f,g] is corroborated by quantum mechanical calculations [58h]. Knudsen effusion mass spectrometry measurements [58i,j,k] confirm that, at T = 2700K, 80%, 14% and 6% of the graphite partial pressure arise respectively from $C_3$, $C_1$ and $C_2$ species. We thus anticipate several species of Carbon to be present in the vapor for our explosion experiments.

The posited explosion mechanism deserves additional discussion. The initial transfer of carbon atoms (or clusters) from the solid to the gas phase is nominally a high temperature process; bulk graphite only sublimes (atmospheric pressure) at T = 3640 +/− 25 °K [58], considerably higher than the average temperature (1800 °K < T < 2400 °K) attained in these explosions. The kinetics are slightly more forgiving. In their classic determination of the heat of vaporization of (monolithic) graphite, Marshall and Norton [59] measured the rate of surface mass loss, e.g. $dm/dt|_{surface} = 1.1 * 10^{-5}$ g/cm$^2$-sec (T = 2800 °K). For a spherical particle, in time Δt, the radius change is $\Delta r = dm/dt|_{surface}\ \Delta t/\rho$. In a characteristic time, Δt ~ 1 msec, this yields Δr ~ 5 nm, which, for primary nanoparticles, can liberate significant carbon into the gaseous phase. We also might expect (due to a large defect density in the highly strained surface) that $dm/dt|_{surface}$ would be higher for the nanoscale allotropes than for the monolithic solid—but these have yet to be measured. Nonetheless, the above estimate still suggests that local hot spots, higher than the global average temperature resulting from the explosion, are required in order to liberate sufficient carbon to sustain the explosion. We note that the adiabatic flame temperature of the chemical igniter, $T_{flame}$~ 3870 °K [60] is higher than the sublimation temperature $T_{sublim}$~ 3640 °K. Thus, material heated by the igniter may be subliming and burning in the gas phase; the igniter serves as the above-hypothesized ‘hot spots’.

### 4.7 Thermodynamics

In [3], we show that explosion overpressure may be successfully estimated from the equilibrium thermodynamics of the reaction 2 C + $O_2$ → 2 CO.

## 5. Conclusion

There is a concern that engineered carbon nanoparticles, when manufactured on an industrial scale, may present an explosion hazard. Explosion testing has been performed on 20 types of carbonaceous particles. These include several different codes of SWCNTs (single-walled carbon nanotubes), MWCNTs (multi-walled carbon nanotubes) and CNFs (carbon nanofibers), graphene, diamond, fullerene, as well as several different control carbon blacks and graphites. Explosion screening was performed in a 20 L explosion chamber, at a concentration of 500 $g/m^3$, using a 5 kJ ignition source. Time traces of overpressure were recorded. Samples typically exhibited $P_m$ ~ 5–7 bar, and $K_{St}$ ~ 10 – 80 bar-m/s, which places [5,54] these materials in European Dust Explosion Class St-1. There was minimal variation between these different materials. The explosive characteristics of these carbonaceous powders are uncorrelated with particle size (BET specific surface area). The carbonaceous nanopowders thus exhibit explosive severities very similar to those of the micron-sized powders. We have argued for a universal mechanism of combustion of these different allotropes. We suggest that carbon atoms are transferred from the solid surface to the gas phase, possibly as a result of the local high temperature provided by the igniter; high temperature oxidation, $2C + O_2 \rightarrow 2CO$, occurs in the gas phase; as the system cools, the CO disproportionates $2CO \rightarrow C$ (soot) + $CO_2$, generating the ubiquitous soot balls observed in the electron micrographs of the exploded material.

## Supplementary Material

Refer to Web version on PubMed Central for supplementary material.

## Acknowledgments

We thank the late K.L. Cashdollar and C.-K. Man (NIOSH) for introducing us to the parameters and measurements necessary to characterize dust explosions. R. Hatfield (Pacific Surface Science) performed the BET specific surface area measurements. We thank M.E. Birch (NIOSH) for helpful discussions, R.H. Hurt (Brown) and an astute referee for helpful comments, and K.E. Ashley, G.S. Earnest, D.E. Evans, A. Garcia, R.P. Streicher (NIOSH) for their careful reading of the manuscript.

This work was supported through the NIOSH Nanotechnology Research Center. We especially thank Paul Schulte (NIOSH) for the prescient recognition of the potential explosion hazard posed by these materials and for the encouragement of this research.

## References

1. Dastidar, AG.; Boilard, S.; Amyotte, PR.; Turkevich, LA. Proceedings 9th Global Congress on Process Safety. San Antonio, TX: AIChE; 2013. Explosibility of nano-sized metal powders. [28 April-1 May 2013]
2. Ajayan PM, Terrones M, de la Guardia A, Huc V, Grobert N, Wei BQ, Lezec H, Rauranath G, Ebbesen TW. Nanotubes in a flash—ignition and reconstruction. Science. 2002; 296:705. [PubMed: 11976446]
3. Turkevich LA, Dastidar AG, Hachmeister Z, Lim M. Potential explosion hazard of carbonaceous nanoparticles: Explosion parameters of selected materials. J. Hazardous Materials. 2015; 295:97–103.
4. Bartknecht, W. Dust Explosions—Course, Prevention, Protection. Berlin: Springer-Verlag; 1989.
5. Eckhoff, RK. Dust Explosions in the Process Industries. 3rd. Elsevier, Burlington, MA: Gulf Professional Publishing; 2003.

6. Abbasi T, Abbasi SA. Dust explosions—cases, causes, consequences, and control. J. Hazardous Materials. 2007; 140:7–44.
7. Morozzo di Bianze, CL. Memoirs of the Academy of Sciences of Turin. Vol. 2. London: Repertory of Arts and Manufactures; 1795. Account of a violent explosion which happened in a flour warehouse, at Turin, December the 14th, 1785, to which are added some observations on spontaneous inflammations; p. 416-432.reprinted with forward by N. Piccinini (Poletecnico di Torino, 1996), cited in [5]
8. CSB. U.S. Chemical Safety and Hazard Investigation Board Report No 2008-05-I-GA. Washington, DC: 2009 Sep. Investigation Report: Sugar Dust Explosion and Fire (14 killed, 36 injured), Imperial Sugar Company, Port Wentworth, Georgia, February 7, 2008.
9. MSHA. U.S. Department of Labor, Mine Safety and Health Administration, Coal Mine Safety and Health Report of Investigation. Arlington, VA: 2011 Dec. Report of Investigation: Fatal Underground Mine Explosion, Aril 5, 2010, Upper Big Branch Mine-South, Performance Coal Company, Montcoal, Raleigh County, West Virginia, ID No. 46-08436.
10. Boilard, S. M.S. thesis: Process Engineering & Applied Science. Halifax, Nova Scotia, CAN: Dalhousie Univ.; 2013. Explosibility of Micron- and Nano-Size Titanium Powders.
11. Wei F, Zhang Q, Qian W-Z, Yu H, Yao W, Luo GH, Xu G-H, Wang D-Z. The mass production of carbon nanotubes using a nano-agglomerate fluidized bed reactor: a multiscale space-time analysis. Powder Technology. 2008; 183:10–20.
12. Zhang Q, Yu H, Liu Y, Qian W, Wang Y, Luo G, Wei F. Few walled carbon nanotube production in large scale by nano-agglomerate fluidized bed process. Nano. 2008; 3:45–50.
13. Zhang Q, Huang J-Q, Zhao M-Q, Qian W-Z, Wei F. Carbon nanotube mass production: principles and processes. Chem. Sus. Chem. 2011; 4:864–889.
14. Vignes, A.; Traore, M.; Dufaud, O.; Perrin, L.; Bouillard, J.; Thomas, D. 8th World Congress of Chemical Engineers. Montreal, Quebec, CAN: 2009 Aug.. Assessing explosion severity of nanopowders with the 20 L sphere; p. 23-27.paper 01350
15. Eckhoff RK. Are enhanced dust explosion hazards to be foreseen in production, processing and handling of powders consisting of nm-particles? Nanosafe 2010: Intl. Conf. on Safe Production and Use of Nanomaterials, J. Phys. Conf. Ser. 2011; 304:1–20.
16. Dufaud O, Vignes A, Henry F, Perrin L, Bouillard J. Ignition and explosion of nanopowders: something new under the dust. NanoSafe 2010: Intl. Conf. on Safe Production and Use of Nanomaterials, J. Phys. Conf. Ser. 2011; 304:012076.
17. Knowles EE. Nanotechnology—evolving occupational safety, health and environmental issues. Professional Safety. 2006 Mar.:20–27. www.asse.org.
18. Pritchard, DK. HSL/2004/12. Buxton, UK: Health and Safety Laboratory; 2004. Literature Review —Explosion Hazards Associated with Nanopowders.
19. Wu HC, Chang RC, Hsiao HC. Research of minimum ignition energy for nano titanium powder and nano iron powder. J. Loss Prev. Process Ind. 2009; 22:21–24.
20. Amyotte PR. Are classical process safety concepts relevant to nanotechnology applications? Nanosafe 2010: International Conf. on Safe Production and Use of Nanomaetrials, J. Phys. Conf. Ser. 2011; 304:1–10.
21. Worsfold SM, Amyotte PR, Khan FI, Dastidar AG, Eckhoff RK. Review of explosibility of nontraditional dusts. Ind. Eng. Chem. Res. 2012; 51:7651–7655. republished as ‘Explosibility of non-traditional dusts’. *Hazardex* (July 2013): 16–23.
22. GESTIS-DUST-EX. http://staubex.ifa.dguv.de/explosuche.aspx, compiled by IFA (Institut fuer Arbeitsschutz der Deutschen Gesetzlichen Unfallversicherung).
23. Faraday M, Lyell C. Report from Messrs. Lyell and Faraday to the Right Hon. Sir James Graham, Bart., Secretary of State for the Home Department, on the subject of the explosion at the Haswell collieries and on the means of preventing similar accidents. Reports from Commissioners: 1845, Vol. 3, page 511. House of Commons, Parliamentary Papers. 1845 Apr 18.16:3–13. *Phil. Mag. Ser. 3* 26 (170): 16-35 (Jan. 1845).
24. Hartmann, I.; Jacobson, M.; Williams, RP. US Bureau of Mines Report 5052. Washington, DC: 1954. Laboratory Explosibility Study of American Coals.
25. Cashdollar KL. Coal dust explosibility. J. Loss Prev. Process Ind. 1996; 9:65–76.

26. Seweryniak M, Maslon J. Konferencja “Sadze Techniczne” (Jaszowiec, Poland) Wyd. NIT i NM Pwr., No. 288, Konferencje. 1985:177–190. cited in [28].
27. Seweryniak M, Kordylewski W, Maslon J, Wysocki L. Wlasnosci Wybuchowe Sadz, Nauka i Technika Pozarnicza. 1989; 1:56–63. cited in [28].
28. Kordylewski W, Seweryniak M. Explosion and flammability properties of furnace carbon blacks. Archivum Combustionis. 1992; 12:153–160.
29. Denkevits A, Dorofeev S. Dust Explosion Experiments: Measurement of Explosion Indices of Graphite Dusts. Report FZKA-6872 Forschungzentrum Karlsruhe GmbH (Karlsruhe). Technik und Umwelt. Inst. fuer Kern- und Energie-technik / Programm Kernfusion. 2003
30. Denkevits A, Dorofeev S. Explosibility of fine graphite and tungsten dusts and their mixtures. J. Loss Prev. Process Ind. 2006; 19:174–180.
31. ASTM E1226. Standard test method for explosibility of dust clouds. West Conshohocken, PA: ASTM International; 2012.
32. Bouillard J, Vignes A, Dufaud O, Perrin L, Thomas D. Explosion risks from nanomaterials. Nanosafe 2008: Intl. Conf. on Safe Production and Use of Nanomaterials, J. Phys. Conf. Series. 2009; 170:012032.
33. Schuster F, Bouillard J. NANOSAFE2: Safe production and use of nanomaterials. European project No. 515843-2. 2005–2009. www.nanosafe2.org.
34. Bouillard, J.; Vignes, A.; Dufaud, O.; Perrin, L.; Thomas, D. AIChE Annual Meeting. Nashville, TN: 2009 Nov.. Safety aspects of reactive nanopowders; p. 8-13.
35. Bouillard J, Vignes A, Dufaud O, Perrin L, Thomas D. Ignition and explosion risks of nanopowders. J. Hazardous Materials. 2010; 181:873–880.
36. Holbrow, P.; Wall, M.; Sanderson, E.; Bennett, D.; Rattigan, W.; Bettis, R.; Gregory, D. HSE RR782. Buxton, UK: Health and Safety Executive; 2010. Fire and Explosion Properties of Nanopowders.
37. Peukert W. Entwicklungstendenzen in der Feststoffverfahrenstechnik [Trends in solids process engineering]. Chemie-Ingenieur-Technik. 1996; 66:1254–1263.
38. Beck, H.; Glienke, N.; Moehlmann, C. Combustion and Explosion Characteristics of Dusts. Sankt Augustin: Benufsgenossenschaftliches Institut fuer Arbeitssicherkeit; 1997.
39. Hertzberg, M.; Cashdollar, KL. STP 958. West Conshohocken, PA: ASTM; 1987. Introduction to dust explosions; Industrial Dust Explosions; p. 5-32.
40. Nagy, J.; Verakis, HC. Development and Control of Dust Explosions. Basel: Marcel Dekker; 1983.
41. Dorsett, HG.; Jacobson, M.; Nagy, J. US Bureau of Mines Report 5624. Washington, DC: 1960. Laboratory Equipment and Test Procedures for Evaluating Explosibility of Dusts.
42. Amyotte PR, Eckhoff RK. Dust explosion causation, prevention and mitigation: an overview. J. Chem. Health & Safety. 2010; 17:15–28.
43. Siwek, R. 20-L Laborapparatus fuer die Bestimmung der Explosionskenngrossen breunbarer Staube [20-liter laboratory apparatus for determination of explosion characteristics of combustible dusts]. Basel, Switz: Ciba-Geigy, AG; Winterthur, Switz: Winterthur Engineering College; 1977.
44. Siwek, RL. Development of a 20 ltr Laboratory Apparatus and its Application for the Investigation of Combustible Dusts. Ciba Geigy, AG: Basel, Switz; 1985.
45. Siwek, RL. Reliable determination of the safety characteristics in 20-L apparatus. Proceedings of the Flammable Dust Explosion Conference; St. Louis, MO. 1988; p. 529-573.
45a. Cashdollar KL, Chatrathi K. Minimum explosible dust concentrations measured in 20-L and 1-m3 chambers. Combustion Sci. Tech. 1992; 87:157–171.
45b. Kalejaiye O, Amyotte PR, Pegg MJ, Cashdollar KL. Effectiveness of dust dispersion in the 20-L Siwek chamber. J. Loss Prev. Process Ind. 2010; 23:46–59.
45c. Dahoe AE, Cant RS, Pegg MJ, Scarlett B. On the transient flow in the 20-liter explosion sphere. J. Loss Prev. Process Ind. 2001; 14:475–487.
45d. Dahoe AE, Cant RS, Scarlett B. On the decay of turbulence in the 20-Lliter explosion sphere. Flow, Turbulence Combustion. 2001; 67:159–184.

45e. Dahoe AE, Zevenbergen JF, Lemkowitz SM, Scarlett B. Dust explosions in spherical vessels: the role of flame thickness in the validity of the ‘cube-root-law’. J. Loss Prev. Process Ind. 1996; 9:33–44.

45f. Cloney, CT.; Ripley, RP.; Amyotte, PR.; Khan, FI. Quantifying the effect of strong ignition sources on particle preconditioning and distribution in the 20-L chamber. Ninth International Symposium on Hazards, Prevention and Mitigation of Industrial Explosions; ISHPMIE; Krakow, POL. 22–27 July 2012; p. 19-25.

45g. Sanchirico R, Russo P, Di Sarli V, Di Benedetto A. Explosibility and flammability characteristics of nicotinic acid-lycopodium/air mixtures. Chem. Eng. Trans. 2014; 36:265–270.

45h. Sanchirico R, Di Benedetto A, Garcia-Agreda A, Russo P. Study of the severity of hybrid mixture explosions and comparison to pure dust-air and vapour-air explosions. J. Loss Prev. Process Ind. 2011; 24:648–655.

45i. Kuai N, Huang W, Du B, Yuan J, Li Z, Gan Y, Tan J. Experiment-based investigations on the effect of ignition energy on dust explosion behaviors. J. Loss Prev. Process Ind. 2013; 26:869–877.

45j. Di Benedetto A, Garcia-Agreda A, Russo P, Sanchirico R. Combined effect of ignition energy and initial turbulence on the explosion behavior of lean gas/dust-air mixtures. Ind. Eng. Chem. Res. 2012; 51:7663–7670.

46. Brunauer S, Emmett PH, Teller E. Adsorption of gases in multimolecular layers. J. Am. Chem. Soc. 1936; 60:309–319.

47. Sing KSW, Everett DH, Haul RAW, Moscou L, Pierotti RA, Rouquerol J, Siemieniewska T. Reporting physisorption data for gas/solid systems with special reference to the determination of surface area and porosity (recommendations 1984). Pure Appl. Chem. 1985; 57:603–619.

48. Adamson, AW. Physical Chemistry of Surfaces. 5th. Vol. chapter XIV-5. Chichester: John Wiley; 1990.

49. Rouquerol J, Avnir D, Fairbridge CW, Everett DH, Haynes JH, Pernicone N, Ramsay JDF, Sing KSW, Unger KK. Recommendation for the characterization of porous solids (technical report). Pure Appl. Chem. 1994; 66:1739–1758.

50. ASTM D6556. Standard test method for carbon black—total and external surface area by nitrogen adsorption. West Conshohocken, PA: ASTM International; 2010.

51. Dahoe AE, Zevenbergen JF, Lemkowitz SM, Scartlett B. Dust explosions in spherical vessels: the role of flame thickness in the validity of the ‘cube-root law’. J. Loss Prev. Process Ind. 1996; 9:33–44.

52. Cashdollar KL. Overview of dust explosibility characteristics. J. Loss Prev. Process Ind. 2000; 13:183–199.

53. Myers, TJ.; White, KC.; Xu, T. Proceedings Mary Kay O’Connor Process Safety Symposium. College Station, TX: 2008. Did a dust explosion occur? Microscopic and thermogravimetric techniques to determine if a dust participated in an explosion event.

54. NFPA 68: Standard on Explosion Protection by Deflagration Venting. Quincy, MA: National Fire Protection Association; 2007.

55. Pyrograf, private communication. 2012

56. Atkins, P.; de Paula, J. Physical Chemistry, Thermodynamics and Kinetics. 9th. Oxford: Oxford Univ. Press; 2009. p. 215

57. Holleman, AF.; Wiberg, E.; Wiberg, N. Inorganic Chemistry. San Diego: Academic Press; 2001. p. 810

58. Hempel, CA., editor. Encyclopedia of the Chemical Elements. Reinhold, New York: 1968. p. 106

58a. Mattauch J, Ewald H, Hahn O, Strassman F. Hat ein Caesium-isotop langer Halbwertszeit existiert? Z. fuer Physik. 1943; 120:598–617.

58b. Brewer L, Gilles PW, Jenkins FA. The vapor pressure and heat of sublimation of graphite. J. Chem. Phys. 1948; 16:797–807.

58c. Chupka WA, Inghram MG. Investigations of the heat of vaporization of graphite. J. Chem. Phys. 1953; 21:371, 1313.

58d. Chupka WA, Inghram MG. Direct determination of the heat of sublimation of Carbon with the mass spectrometer. J. Phys. Chem. 1955; 59:100–104.

58e. Glockler G. The heat of sublimation of graphite and the composition of Carbon vapor. J. Chem. Phys. 1954; 22:159–161.

58f. Doernenburg E, Hintenberger H. Das Auftreten vielatomiger Kohlenstoffmolukuele im Hochfrequensfunken zwischen Graphitelektroden. Z. Naturforsch. 1959; 14A:765–767.

58g. Doernenburg E, Hintenberger H. Ueber der Struktur der im Hochfrequensfunken entstehenden vielatomigen Kohlstoffmolekuele. Z. Naturforsch. 1961; 16A:532–534.

58h. Pitzer KS, Clemente E. Large molecules in carbon vapor. J. Am. Chem. Soc. 1959; 81:4477–4485.

58i. Gingerich KA. The enthalpy of formation of the $C_7$ molecule from mass spectrometric equilibrium measurements. Chem. Phys. Lett. 1992; 196:245–248.

58j. Gingerich KA, Finkbeiner HC, Schmude RW Jr. The enthalpy of formation of the C6 molecule from mass spectrometric equilibrium measurements. Chem. Phys. Lett. 1993; 207:23–26.

58k. Gingerich KA, Finkbeiner HC, Schmude RW Jr. Enthalpies of formation of small linear carbon clusters. J. Am. Chem. Soc. 1994; 116:3884–3888.

59. Marshall AL, Norton FJ. Carbon vapor pressure and heat of vaporization. J. Am. Chem. Soc. 1950; 72:2166–2171.

60. Hertzberg M, Cashdollar KL, Zlochower IA. Flammability limit measurements for dusts and gases: ignition energy requirements and pressure dependences. Symp. (International) on Combustion (Proc. Combustion Institute) 21. 1988:303–313.

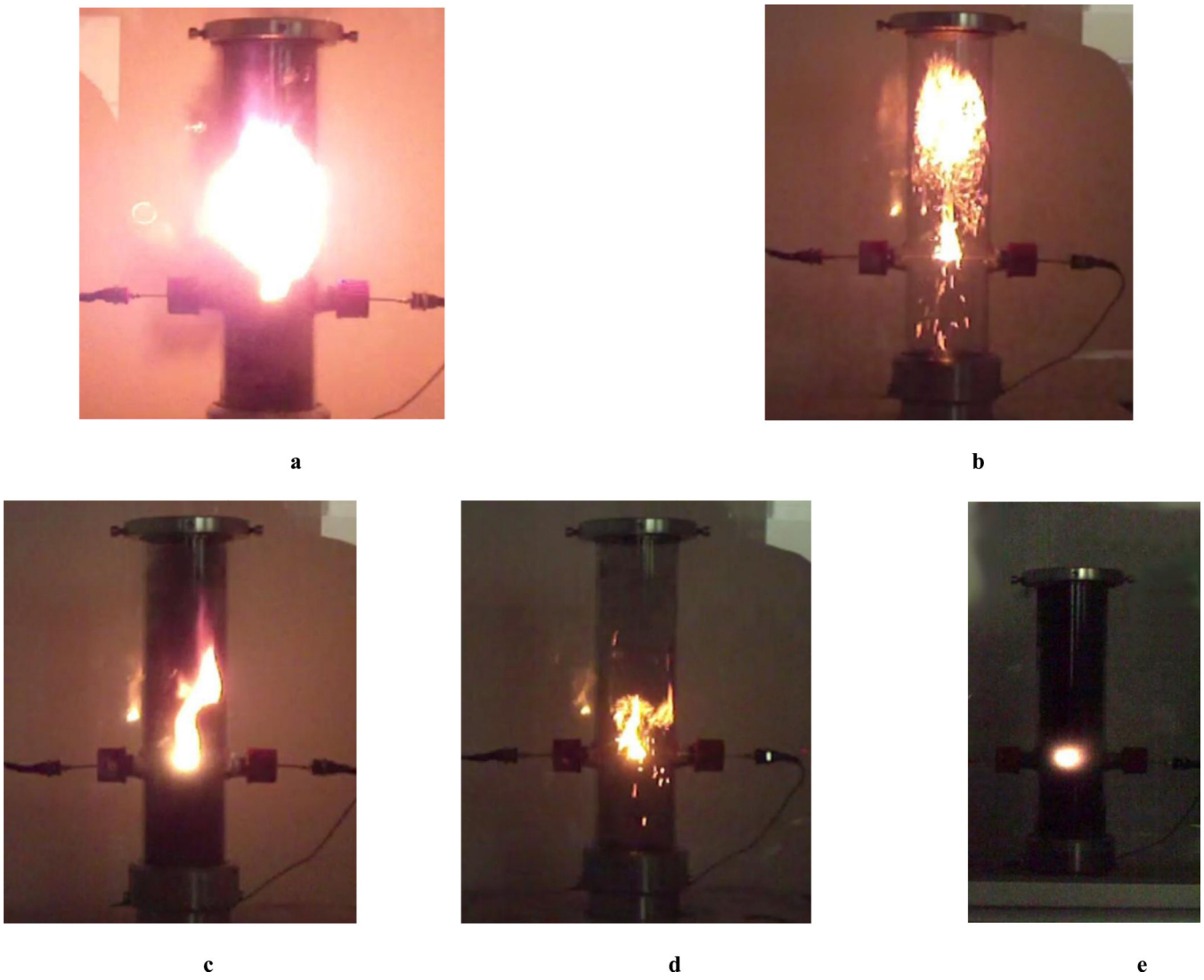


**Figure 1.**
Explosion of different SWCNTs in Hartmann tube configuration: a) Unidym; b) Unidym (hexane extracted); c) SWeNT; d) CheapTubes; e) similar explosion of fullerene.

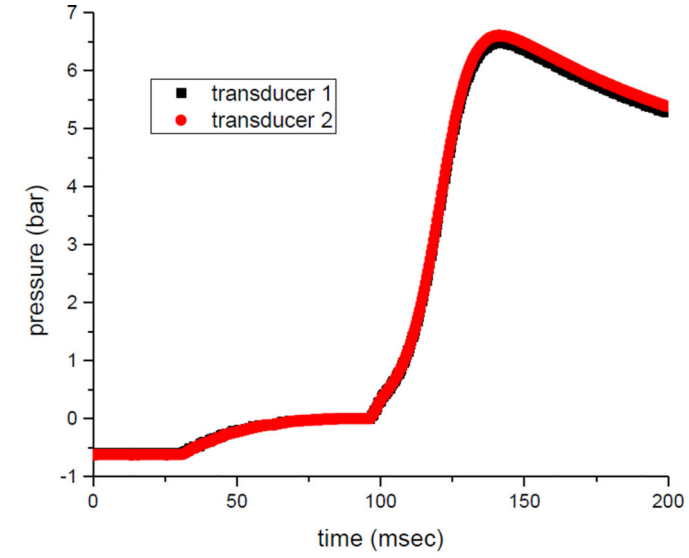


**a**

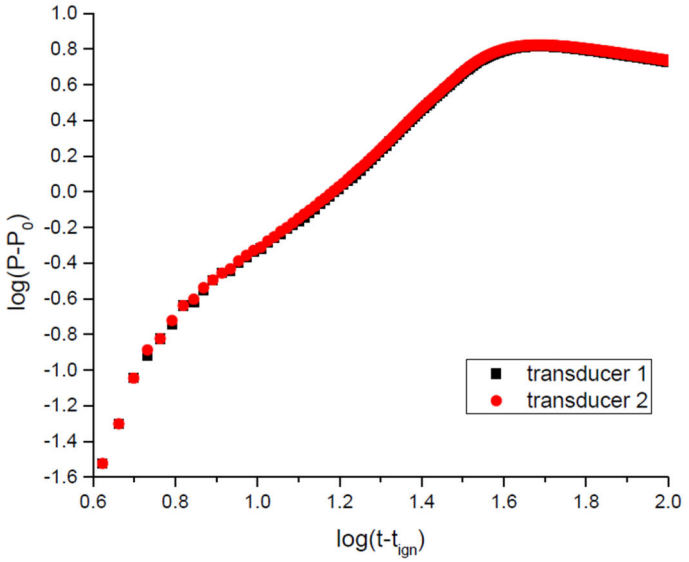


**b**

**Figure 2.**

a) Experimental time trace of over-pressure, $P - P_0$, for the explosion of a SWCNT (CheapTubes).

b) Double logarithmic plot of time trace a).

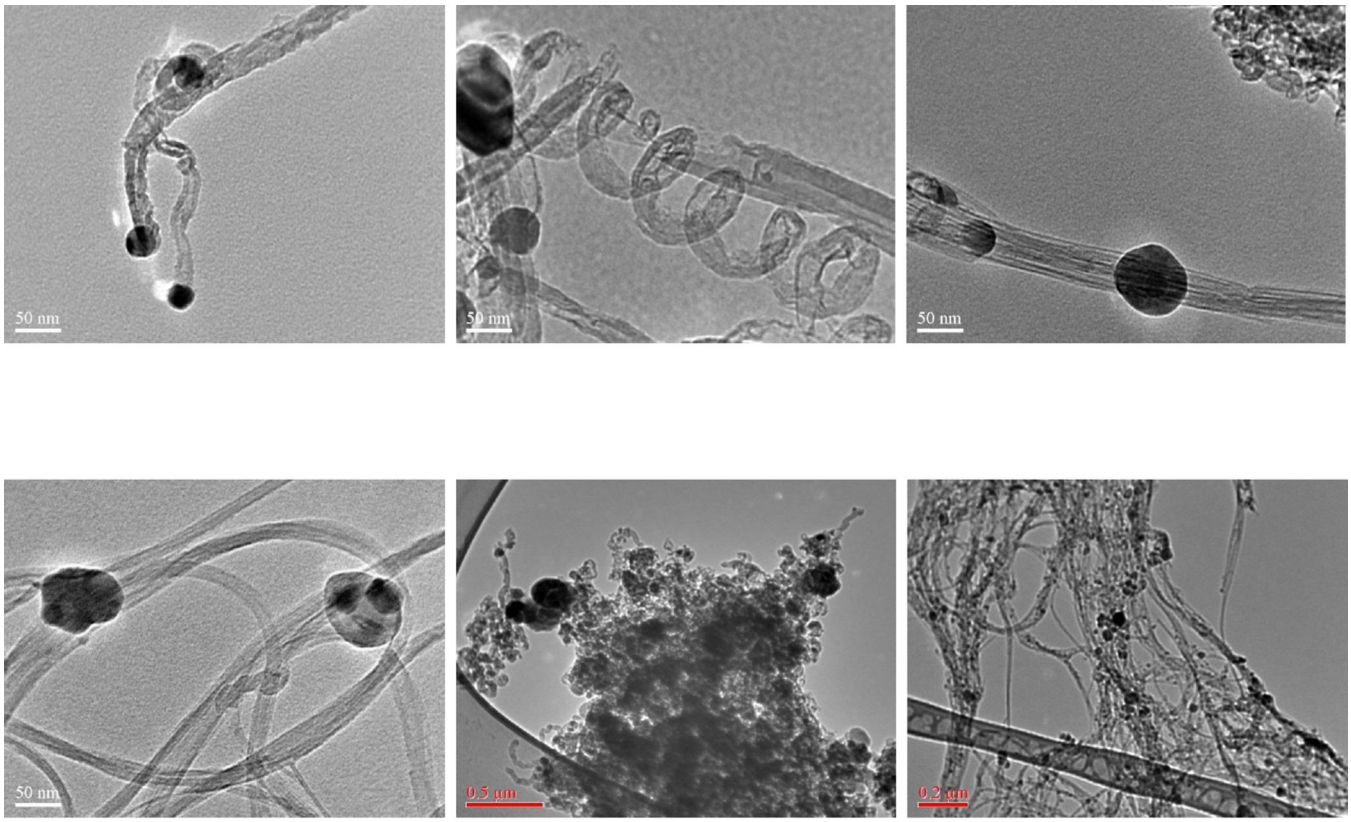


**a) – f)**

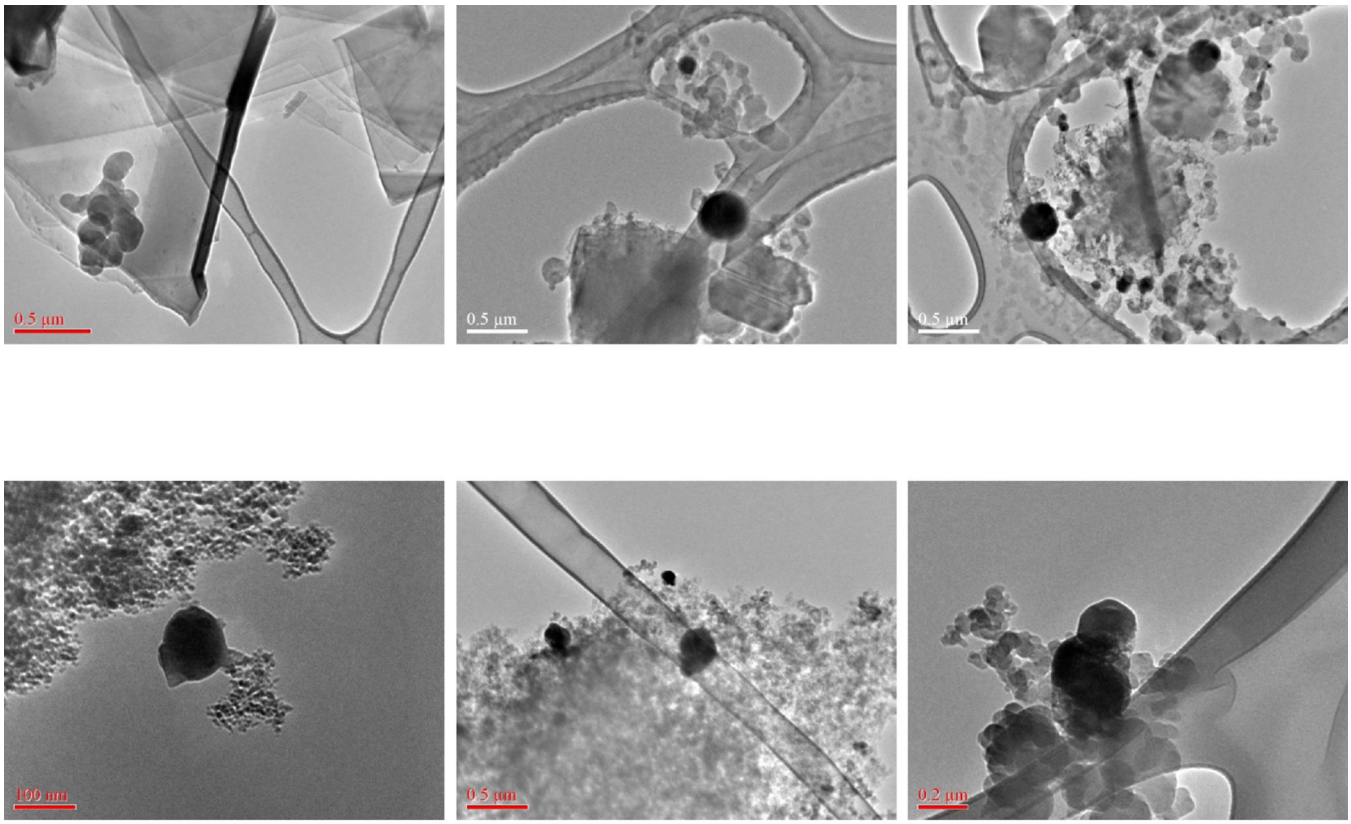


**g)-l)**

**Figure 3.**

TEM micrographs of exploded carbonaceous naomaterials: a)–b) MWCNT; c)–d) SWCNT (CheapTubes); e) SWCNT (SWeNT); f) SWCNT (Unidym HiPCO); g) graphene; h)–i) fullerene; j) 10 nm diamond; k) carbon black (Printex 90); l) carbon black (Sterling V).

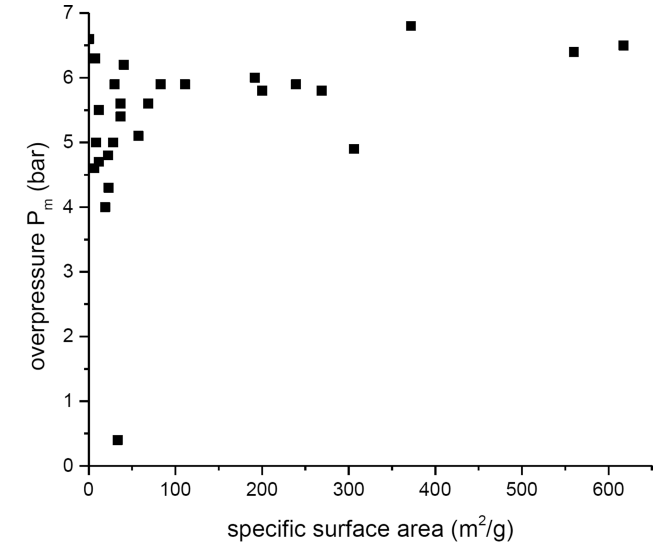


**a**

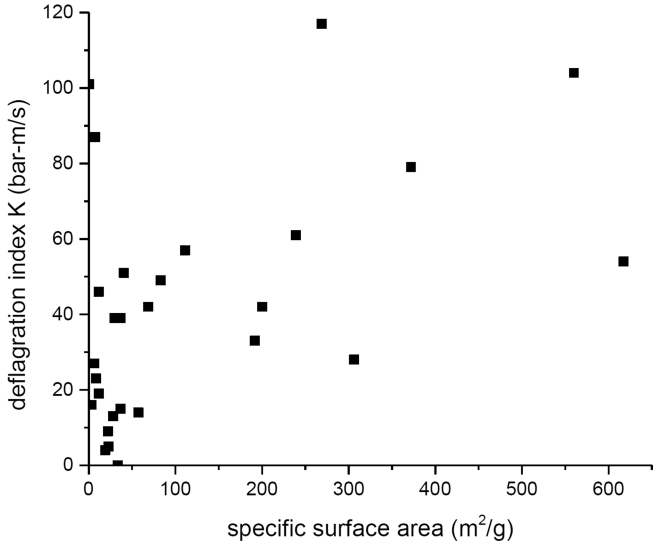


**b**

**Figure 4.**

Relation of screening explosion parameters to BET specific surface area: a) $P_m$ ; b) $K = V^{1/3} dP/dt|_m$.

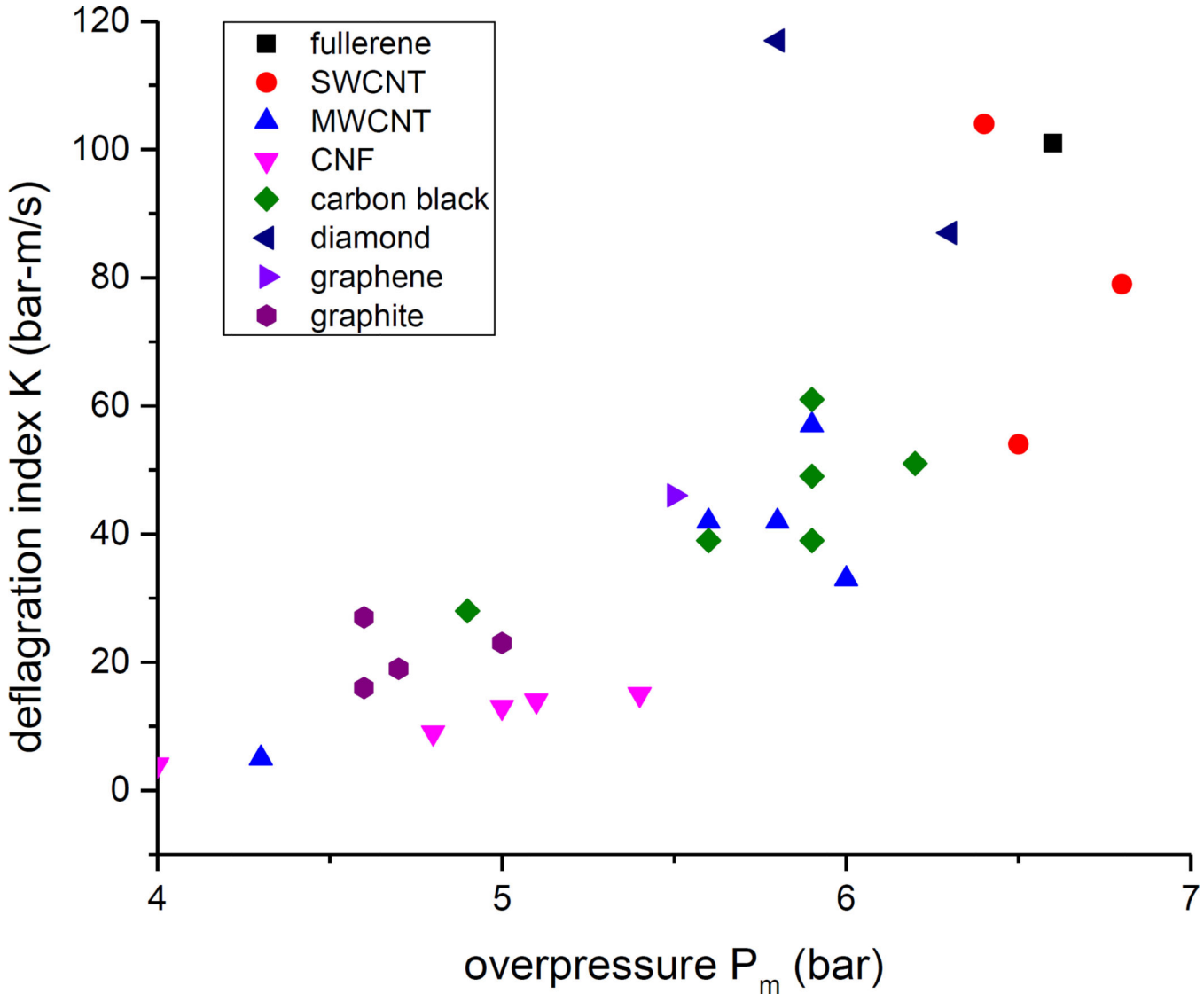


**Figure 5.**
Correlation of the kinetic explosion parameter, K, with the thermodynamic explosion parameter, $P_m$.

**Table 1**

Literature explosion parameters for carbonaceous nanomaterials.

| **Material** | | | **$d_{pr\ part}$** | **$d_{agg}$** | **BET** | **$P_{max}$** | **$dP/dt|_{max}$** | **$K_{St}$** | **MEC** | **MIE** | **$MIT_{cloud}$** | **$MIT_{layer}$** | **$T_{onset}$** | **reference** |
|---|---|---|---|---|---|---|---|---|---|---|---|---|---|---|
| | | | **[nm]** | **[μm]** | **[$m^2$/g]** | **[bar]** | **[bar/s]** | **[m-bar/s]** | **[g/$m^3$]** | **[J]** | **[°C]** | **[°C]** | **[°C]** | |
| Furnace Carbon Blacks | | | | | | | | | | | | | | |
| | | Vulcan | | | | 8.5 | 24 | 7 | 60 | | | | | 32 |
| | | Vulcan (P) | | | | 9.1 | 62 | 17 | 60 | | | | | 32 |
| | | unspecified | | | | 9.4 | 122 | 33 | 60 | | | | | 62 |
| | | unspecified | | | | 10.0 | 65 | 17 | 50 | | | | | 63 |
| Channel & Special Blacks | | | | | | | | | | | | | | |
| | | SAO | | | | 5.6 | 68 | 19 | 86 | | | | | 33 |
| | | SAB-1 | | | | 6.0 | 73 | 20 | 68 | | | | | 33 |
| | | SAB-1 (P) | | | | 5.2 | 69 | 19 | 43 | | | | | 33 |
| | | SAGAL-3 (P) | | | | 6.0 | 83 | 23 | 50 | | | | | 33 |
| | | SAKAP-6 | | | | 6.1 | 82 | 22 | 62 | | | | | 33 |
| Brown Coal | | | 32 | | | 11.0 | 152 | 41 | 60 | | | | | 34 |
| Carbon Blacks | | | | | | | | | | | | | | |
| | semiactive | Sapex 20 | 89 | | 27.0 | 6.0 | 79 | 22 | 150 | | 885 | 395 | | 34 |
| | | Sapex 20 (P) | 89 | | 26.5 | 6.1 | 63 | 18 | 144 | | 882 | 435 | | 34 |
| | | Sapex 35 | 78 | | 36.9 | 6.8 | 66 | 19 | 126 | | | 359 | | 34 |
| | | Sapex 35 (P) | 78 | | 39.5 | 6.1 | 50 | 14 | 103 | | 896 | 415 | | 34 |
| | active N330 | Carbex 330 | 33 | | 70.0 | 6.4 | 103 | 29 | 71 | | 683 | 360 | | 34 |
| | | Carbex 330 (P) | 32 | | 81.2 | 6.3 | 96 | 27 | 75 | | 683 | 410 | | 34 |
| | | Carbex 330a | 30 | | 85.0 | 6.3 | 182 | 51 | 66 | | 667 | 350 | | 34 |
| | | Vulcan 3 | 30 | | 81.0 | 6.3 | 169 | 47 | 73 | | 656 | 450 | | 34 |
| | active N200 | Vulcan 6 | 24 | | 122.0 | 6.9 | 246 | 69 | 61 | | 645 | 470 | | 34 |
| Graphite | | | | | | | | | | | | | | |
| | | fine | | 4 | | 6.5 | 260 | 73 | 70 | $10^3$–$10^4$ | | | | 36 |

| **Material** | | | **$d_{pr\ part}$** | **$d_{agg}$** | **BET** | **$P_{max}$** | **$dP/dt|_{max}$** | **$K_{St}$** | **MEC** | **MIE** | **$MIT_{cloud}$** | **$MIT_{layer}$** | **$T_{onset}$** | **reference** |
|---|---|---|---|---|---|---|---|---|---|---|---|---|---|---|
| | | | **[nm]** | **[μm]** | **[$m^2$/g]** | **[bar]** | **[bar/s]** | **[m-bar/s]** | **[g/$m^3$]** | **[J]** | **[°C]** | **[°C]** | **[°C]** | |
| | | coarse-1 | | 25–32 | | 6.0 | 90 | 24 | 100 | $2*10^3$–$10^4$ | | | | 36 |
| | | coarse-2 | | 40–45 | | 6.0 | 75 | 20 | 100 | $2*10^3$–$10^4$ | | | | 36 |
| Carbon Blacks | | | | | | | | | | | | | | |
| | | Corax N115 | | | 150 | 7.5 | 503 | 136 | 60 | $> 10^{-3}$ | | | 405 | 20 |
| | | Corax N550 | | | 50 | 6.7 | 240 | 65 | 60 | $> 10^{-3}$ | | | 460 | 20 |
| | | Thermal Black N990 | | | 20 | 7.2 | 343 | 93 | 60 | $> 10^{-3}$ | | | 510 | 20 |
| | | Printex XE2 | | | 200 | 6.6 | 227 | 62 | 60 | $> 10^{-3}$ | | | 450 | 20 |
| Carbon Nanotube | (MWCNT) | (Arkema) | | | 950 | 7.7 | 326 | 88 | 60 | $> 10^{-3}$ | | | 390 | 20 |

**Table 2**

Screening explosion parameters for carbonaceous nanomaterials (this study).

| **Allotrope** | **Material** | **A** | **$\sigma_A$** | **$P_m(500)$** | **$dP/dt|_m(500)$** | **K(500)** |
|---|---|---|---|---|---|---|
| | | **[$m^2$/g]** | **[$m^2$/g]** | **[bar]** | **[bar/s]** | **[bar-m/s]** |
| diamond | 1 μ | 7.5 | 0.0 | 6.3 | 320 | 87 |
| | 10 nm | 268.9 | 1.2 | 5.8 | 430 | 117 |
| fullerene | $C_{60}$ | 0.4 | 0.0 | 6.6 | 373 | 101 |
| SWCNT | CheapTubes | 372.0 | 3.1 | 6.8 | 290 | 79 |
| | UnidymHiPCO | 559.9 | 8.4 | 6.4 | 382 | 104 |
| | SWeNT SG-65 | 617.2 | 3.0 | 6.5 | 198 | 54 |
| MWCNT | BayTubes C150P | 200.2 | 0.9 | 5.8 | 155 | 42 |
| | BayTubes C150HP | 191.9 | 1.0 | 6.0 | 120 | 33 |
| | Mitsui 7 | 23.0 | 0.5 | 4.3 | 19 | 5 |
| | CheapTubes A | 111.1 | 0.6 | 5.9 | 210 | 57 |
| | CheapTubes B | 68.7 | 0.7 | 5.6 | 156 | 42 |
| CNF (Pyrograf) | PR-19-XT-PS | 28.2 | 0.4 | 5.0 | 47 | 13 |
| | PR-19-XT-LHT | 22.2 | 0.1 | 4.8 | 33 | 9 |
| | PR-19-XT-HHT | 18.9 | 0.3 | 4.0 | 16 | 4 |
| | PR-24-XT-PS | 57.3 | 0.5 | 5.1 | 53 | 14 |
| | PR-24-XT-LHT | 36.8 | 0.3 | 5.4 | 56 | 15 |
| | PR-24-XT-HHT | 33.3 | 0.5 | 0.4 | 0 | 0 |
| carbon black (Cabot) | Regal 330R | 83.0 | 0.3 | 5.9 | 180 | 49 |
| | Monarch 120 | 29.9 | 0.1 | 5.9 | 144 | 39 |
| | Monarch 280 | 40.6 | 0.2 | 6.2 | 188 | 51 |
| | Monarch 900 | 239.2 | 0.9 | 5.9 | 223 | 61 |
| | Sterling V | 36.8 | 0.1 | 5.6 | 142 | 39 |
| carbon black (DeGussa-Huels) | Printex 90 | 306.3 | 4.5 | 4.9 | 103 | 28 |
| graphene (Angstron) | N008-100N | 11.6 | 0.1 | 5.5 | 168 | 46 |
| graphite (Alfa Aesar) | crystalline (300 mesh) | 11.6 | 0.1 | 4.7 | 72 | 19 |

| Allotrope | Material | A | $\sigma_A$ | $P_m(500)$ | $dP/dt\|_m(500)$ | K(500) |
|---|---|---|---|---|---|---|
| | | [$m^2/g$] | [$m^2/g$] | [bar] | [bar/s] | [bar-m/s] |
| | flake (7–10 μ) | 8.4 | 0.1 | 5.0 | 87 | 23 |
| | synth. cond. (325 mesh) | 3.3 | 0.1 | 4.6 | 57 | 16 |
| | natural crystal (2–15 μ) | 6.5 | 0.1 | 4.6 | 98 | 27 |